LATITUDINAL DISTRIBUTION OF AURORAL KILOMETRIC RADIATION BASED ON POLAR SPACECRAFT OBSERVATIONS

C. K. Louis[1†*], K. D. Smith[1†], C. M. Jackman[1], A. R. Fogg[1], J. E. Waters[2], E. P. O'Dwyer[1], and L. Granroth[3]

[†]these authors contributed equally to this work

[*]Corresponding author: corentin.louis@dias.ie

Citation:
Louis, Smith et al., 2023, Latitudinal distribution of Auroral Kilometric Radiation based on Polar spacecraft observations, *in Planetary, Solar and Heliospheric Radio Emissions IX, edited by C. K. Louis, C. M. Jackman, G. Fischer, A. H. Sulaiman, P. Zucca, published by DIAS, TCD*, pp. 125–137, doi: 10.25546/103088

Abstract

Auroral Kilometric Radiation (AKR) is a terrestrial radio emission that occurs above the poles. It is produced by the cyclotron maser instability at frequencies close to the electron cyclotron frequency (proportional to the magnetic field amplitude). The *Polar* orbiter sampled radio emissions from pole to pole for two years, thus AKR emissions were sampled across a broad range of latitudes. This is important because the frequency and visibility of AKR emissions depend on observer latitude. In order to distinguish AKR emissions from other radio sources present in the *Polar* dataset, we used the "SPectrogram Analysis and Cataloguing Environment" (SPACE) labelling tool to create a labeled catalogue, focusing initially on 45 days of *Polar* data, but laying the ground for future examination of this rich dataset, including the application of machine learning approaches using our labels as a training set to classify a broader range of data. From this catalogue we derived occurrence and intensity distributions relative to frequency and observer latitude. These distributions allow constraints to be put on the viewing effects, which is critical to enable robust study of the underlying physics of AKR emission.

[1] *School of Cosmic Physics, DIAS Dunsink Observatory, Dublin Institute for Advanced Studies, Dublin 15, Ireland*
[2] *Aix Marseille Université, CNRS, CNES, LAM, Marseille, France*
[3] *Department of Physics and Astronomy, University of Iowa, Iowa City, IA 52242 USA*

1 Introduction

Auroral Kilometric Radiation (AKR) is the most intense radio emission from Earth's magnetosphere–ionosphere system, and was first observed by Dunckel et al. (1970). AKR correlates well with the intensity of auroral emissions (in optical wavelengths), as they are both excited by the same particle acceleration regions (Gurnett, 1974; Benson & Calvert, 1979; Green et al., 1979; Benson et al., 1980; Huff et al., 1988). AKR has also been shown to be well correlated with the Auroral Electrojet (AE) index (Dunckel et al., 1970; Gurnett, 1974; Voots et al., 1977) and to be an indicator of substorm activity (Morioka et al., 2007, 2011, 2014; Waters et al., 2022). At substorm onset, when reconnection begins in the magnetotail, energetic particles are injected down magnetic field lines towards the poles. These particles either precipitate into the ionosphere, exciting the aurora, or undergo magnetic mirroring and return to the plasma cavity. In this region, there is not enough plasma to contain the energy of the particles (e.g., Treumann & Baumjohann, 2020), and so they emit their energy in the form of AKR. AKR can therefore serve as an excellent diagnostic tool for the study of energy release in Earth's magnetosphere.

The AKR is generated by the cyclotron maser instability (CMI) at a frequency close the electron cyclotron frequency f_{ce} (frequency proportional to the local magnetic field and thus inversely proportional to source altitude), and at the very site of particle acceleration (Wu & Lee, 1979; Le Queau et al., 1984b,a; Pritchett, 1986; Wu, 1985; Treumann, 2006). AKR extends from $\sim$ 30 to 800 kHz, with its main band in the 100-400 kHz range, and a maximum intensity peaking at $\sim$ 200 kHz (Gurnett, 1974) and powers up to 10^9 W (Gurnett, 1974; Zhao et al., 2019). Monitoring the occurrence of AKR bursts and their extension below the 100 kHz main band lower limit (called Low Frequency Extensions, LFEs), allows to probe the intense acceleration of particles and the displacement of radio sources to higher altitudes (Morioka et al., 2007). This allows us to probe magnetospheric activity in the context of space weather, with the ultimate goal of evolving a new geomagnetic index using AKR as a tracer of magnetospheric activity

The radio emissions from the AKR are produced in a very anisotropic manner. Indeed, as they are produced from the CMI, they are emitted along the edges of a hollow conical sheet. Moreover, since the sources of these emissions are located inside cavities where the plasma density is lower than in the surrounding environment (Calvert, 1981; Ergun et al., 1998; Hilgers, 1992; Johnson et al., 2001; Mutel et al., 2003, 2004, 2008), these emissions are subject to strong refraction effects. It is therefore very important to have a good understanding and knowledge of the visual effects to which its emissions are subject (Fogg et al., 2022). For example, one known effect is the local time variation in AKR power, with a preference in the dusk to midnight local time sector with power several orders of magnitude higher than on the dayside (Fogg et al., 2022; Waters et al., 2022). A second known effect is the existence of an equatorial shadow zone (Gurnett, 1974; Lamy et al., 2010; Morioka et al., 2011), extending from about 40^o magnetic latitude at 3 R_E to about 10^o magnetic latitude at 10 R_E, caused by refraction of the AKR on the edges of the plasmasphere.

Spacecraft such as Wind, STEREO, Cluster, Geotail and *Polar* carry radio instruments which allow us to track the intensity and frequency response of the AKR to dynamic space weather. The very elliptical and tilted orbit of the *Polar* spacecraft (see Section 2) allows the entire latitude range to be probed, unlike the Cassini and Wind space missions for example (see Lamy et al., 2010; Waters et al., 2021, for partial distributions of AKR power as a function of latitude). From this observation, building a catalogued database of radio emissions (see Sections 3 and 4) makes it possible to study the visibility effects of the AKR (see Section 5).

2 Dataset

Polar is a NASA satellite launched on February 24$^{\mathrm{th}}$ 1996 in a highly elliptical and tilted orbit (86°) with a perigee at 1.8 R_E (mean Earth radius R_E = 6371 km) and an apogee at 9.0 Earth radii (see Figure 1), with a period of around 18 hours. Perigee was initially over the southern auroral region, but the spacecraft precessed 16° annually post-launch until the end of the mission in 2008 April 28$^{\mathrm{th}}$.

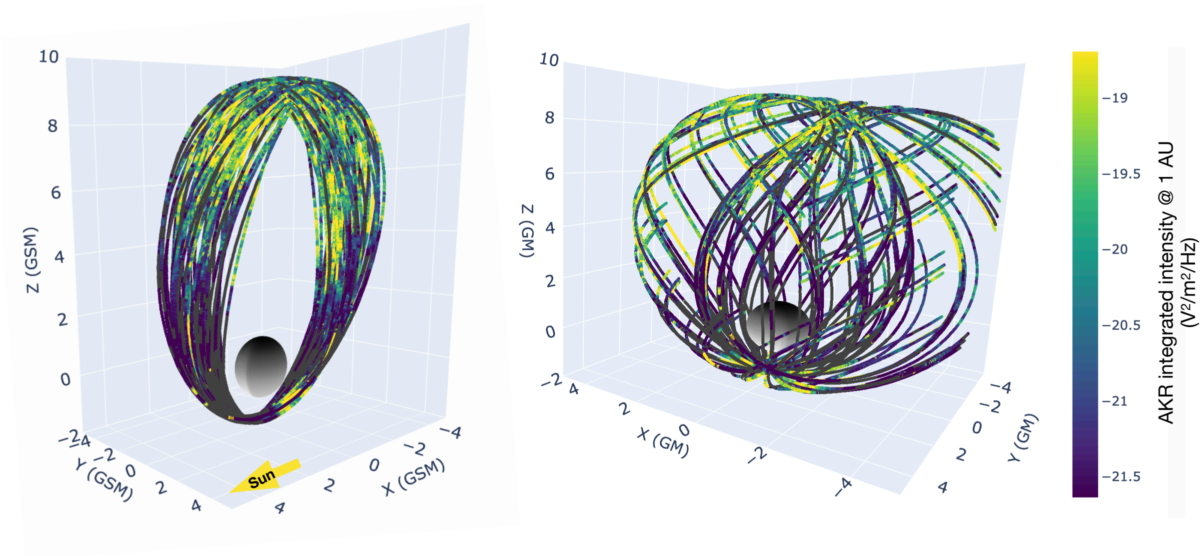

Figure 1: *Trajectory of the* ~ 60 *orbits studied in this article, from 1996 March 25*$^{\mathrm{th}}$ *to 1996 May 9*$^{\mathrm{th}}$ *relative to the Earth (in gray). The Geocentric Solar Magnetospheric (GSM) system in units of Earth radii is used in the left panel, where x is positive sunward, y is defined to be perpendicular to the Earth's magnetic dipole, and z is positive northward. The Geomagnetic (GM) coordinate system is used in the right panel, where Z-axis points to the Geomagnetic north pole, X-axis is in the Earth's magnetic equatorial plane but is fixed with the rotation of the Earth, and Y-axis completes the triad. The magnetic field model used to compute the ephemeris is the International Geomagnetic Reference Field (IGRF) model version 13. The colour of the orbit is the integrated intensity of all labeled emission (excluding "LFE") across all frequencies measured by the PWI instrument (see Table 1 for more details on the labeled features). Two gifs showing these 3D plots from different angles are provided in the online supplementary document of Smith et al. (2022a).*

The "Plasma Waves Investigation" (PWI, Gurnett et al., 1995) onboard is used to detect the electric and magnetic fields of plasma waves, and was operational until 1997 September 16$^{\mathrm{th}}$. The measure of the electric field is done over a frequency range between 0.1 Hz and 800 kHz by a pair of orthogonal two-sphere electric antennas in the spin plane of the spacecraft with sphere–to–sphere separations of 100 meters and 130 meters respectively; and by a short two-sphere electric antenna aligned along the spacecraft spin axis with a sphere–to–sphere separation of 14 meters. For this study, we used data from two on-board sub-receivers that probe frequencies from 12.5 kHz to 800 kHz, with logarithmic spacing. In addition we also used the measurements of the "Magnetic Field Experiment" (Russell et al., 1995) to obtain the local magnetic field amplitude B to infer the electron cyclotron gyro-frequency $\omega_{\rm ce} = 2\pi f_{\rm ce} = eB/m_e$ (with e and m_e the charge and mass of an electron, respectively).

We decided to use *Polar*/PWI observations because of its highly elliptical $\sim$ 18-hour orbits, which allow us to sample views (e.g., over the poles) not sampled by any other spacecraft, almost three times every two days. Figure 1 displays the 60 orbits of *Polar* studied here ($\sim$ 45 days) in the Geocentric Solar Magnetospheric (GSM, left panel) and Geomagnetic (GM, right panel) coordinates system. These orbits allow emissions to be observed at all longitudes (see Figure 1 right panel), different local times (mainly between 2200 and 0100 on the night side and between 1000 and 1400 on the day side, see Figure 1 left panel) and at all latitudes in a very short time. It is thus possible to follow the emissions caused by the same event from several viewpoints. It is however important to note that the spacecraft samples the southern hemisphere at very short distance compared to the measurements in the northern hemisphere. Therefore, less emissions are observed in the southern hemisphere observations of *Polar*, as visible in Figure 1.

3 Method

To label the emissions of interest, the "SPectrogram Analysis and Cataloguing Environment (SPACE)" was used (Louis et al., 2022a,b). SPACE is a visual inspection based emissions labelling software. This approach allows for rapid and accurate manual labelling of temporal–spectral data. The outputs of this labelling tool is a catalogue of labeled temporal–spectral features following the "Time–Frequency Catalogue" (TFCat) specifications, such as their type, their properties (e.g., names and descriptions), their temporal and spectral extents (Cecconi et al., 2023).

For the labelling of the *Polar*/PWI data, three new main features were introduced to the SPACE labelling tool. Firstly, since the *Polar*/PWI radio instrument is composed of several sub-receivers, the tool was updated to allow for data from multiple sub-receivers to be concatenated and presented to the user. Secondly, a toggleable 1D time series overplotting feature was added to overplot the electron cyclotron frequency ($f_{\rm ce}$) value, as calculated from magnetic field measurements by the spacecraft, corresponding to the theoretical frequency of the emissions (see variable dashed-white line in Figure 2). Finally, an option has been implemented to draw horizontal line(s) on the visualisation window at specified frequencies, to aid in interpreting the plot. The lines can be toggled using check boxes (see horizontal dashed-white line at 10^5 Hz in Figure 2).

Spectroscopic data were interpolated and averaged from an original cadence of $\sim$ 2.36 seconds to a cadence of 15 seconds to reduce the computational load (see Smith et al., 2022b,

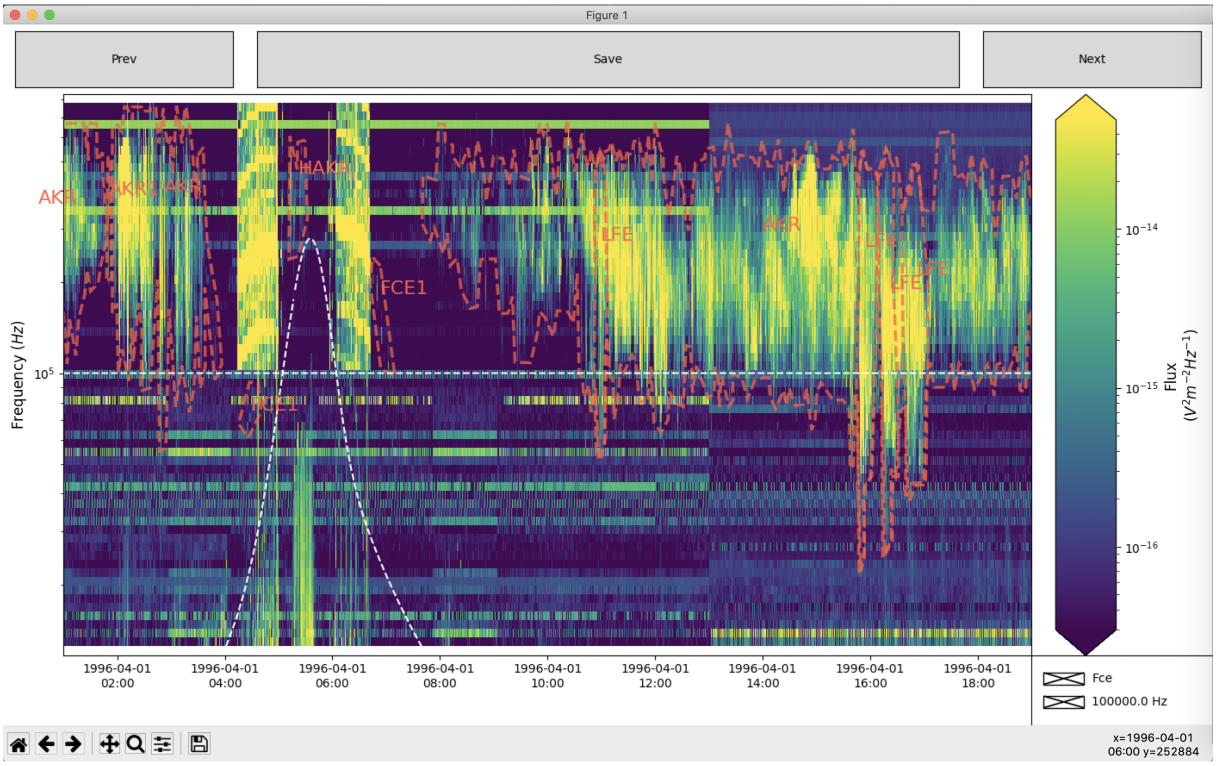

Figure 2: *View of the SPACE labelling tool displaying PWI data on 1996 April 1st from 01:00 to 19:00. The four categories of AKR emission alongside manually drawn emission selections are visible. Saturation effects (potentially due to radiation belts) as Polar approaches perigee are also visible. Data observed within these saturation effects were typically ignored due to their low quality, leading to a systematic bias in recorded emissions. The horizontal dashed-white line at* 10^5 *Hz helps to identify and label the "LFE" features. The variable white-dashed line (Fce) corresponds to the electron cyclotron frequency* $f_{\rm ce}$ *deduced from the magnetic field measurement and helps to identify and label the "FCE" features.*

for the processed dataset and corresponding ephemeris). The data were displayed in windows of 18 hours, corresponding to a slightly longer window than the orbit period of the spacecraft (see Figure 2). The time and frequency of the labeled data is saved to a file which can then be analysed by the user.

4 Auroral Kilometric Radiation database

Emission from AKR was labeled and catalogued into four feature types (see Table 1). The dynamic spectrum displayed Figure 2 shows an example of each feature: one "HAKR" label is visible during the perigee at $\sim$ 05:15–05:45 between $\sim 3 \times 10^5$ and 5×10^5 Hz; two "FCE" labels are visible before and after the perigee at $\sim$ 04:15 between $\sim 6 \times 10^4$ and 9×10^4 Hz, and at $\sim$ 07:00 between $\sim 10^5$ and 2×10^5 Hz; "AKR" labeled emissions are visible throughout the observations; four "LFE" labels are observed during the second half of the observations (e.g., three examples around 16:00).

The data from *Polar* displays a number of saturation effects, radio frequency interference, and datagaps which sometimes made labeling features difficult or impossible, thus some-

Table 1: *List of features labeled using the SPACE labelling tool*

Feature	Description
Auroral Kilometric Radiation (AKR)	Radio emission observed between 30 and 800 kHz
Low Frequency Extension (LFE)	Rapid extensions of the main band of AKR to frequency $\sim$ 30 kHz or lower (contains main band + extension)
High latitude AKR (HAKR)	High latitude AKR, typically observed between 650 kHz and 800 kHz near perigee, separate from AKR
Electron Cyclotron Frequency (FCE)	Emission observed near/parallel to the value of the local electron cyclotron frequency. Emission interpreted as an in situ crossing (or very close observation) of AKR sources near perigee

times potential sources were not labeled or labeled with a quality flag indicating spurious data (indicated with a “1” in their labels, e.g., “AKR1”, “FCE1”, see Figure 2).

Thus far $\sim$ 45 days of data from the start of the observing window has been labeled. The catalogue contains 1251 features sampling $\sim$ 60 orbits and is accessible online (Smith et al., 2022a).

The catalogue follows the TFCat requirements and is then easy to load and read using the TFCat package (Cecconi et al., 2023).

5 Frequency vs. latitudinal distribution of AKR

One of the main scientific results obtained directly from this catalogue is the first complete latitude vs. frequency intensity distribution of AKR emission, displayed in Figure 3. Each panel represents one of the four different feature types listed in Table 1. The coordinate system used here is GSM for the reason that CMI radio emissions are produced at the electron cyclotron frequency which is proportional to the local magnetic field amplitude B. Therefore, the distribution of CMI emissions should be better organised according to magnetic latitude (as observed at Jupiter by Louis et al., 2021). Next to each latitude vs. frequency intensity distribution is plotted an histogram of the latitudinal occurrence of the observation. Occurrences of less than 1 minute (i.e. four 15 second observations in the histograms) should be treated with caution, as the average intensity is calculated over a very small number of events, and is therefore only weakly reliable.

The fact that some components are not observed at all at certain latitudes (e.g., no HAKR

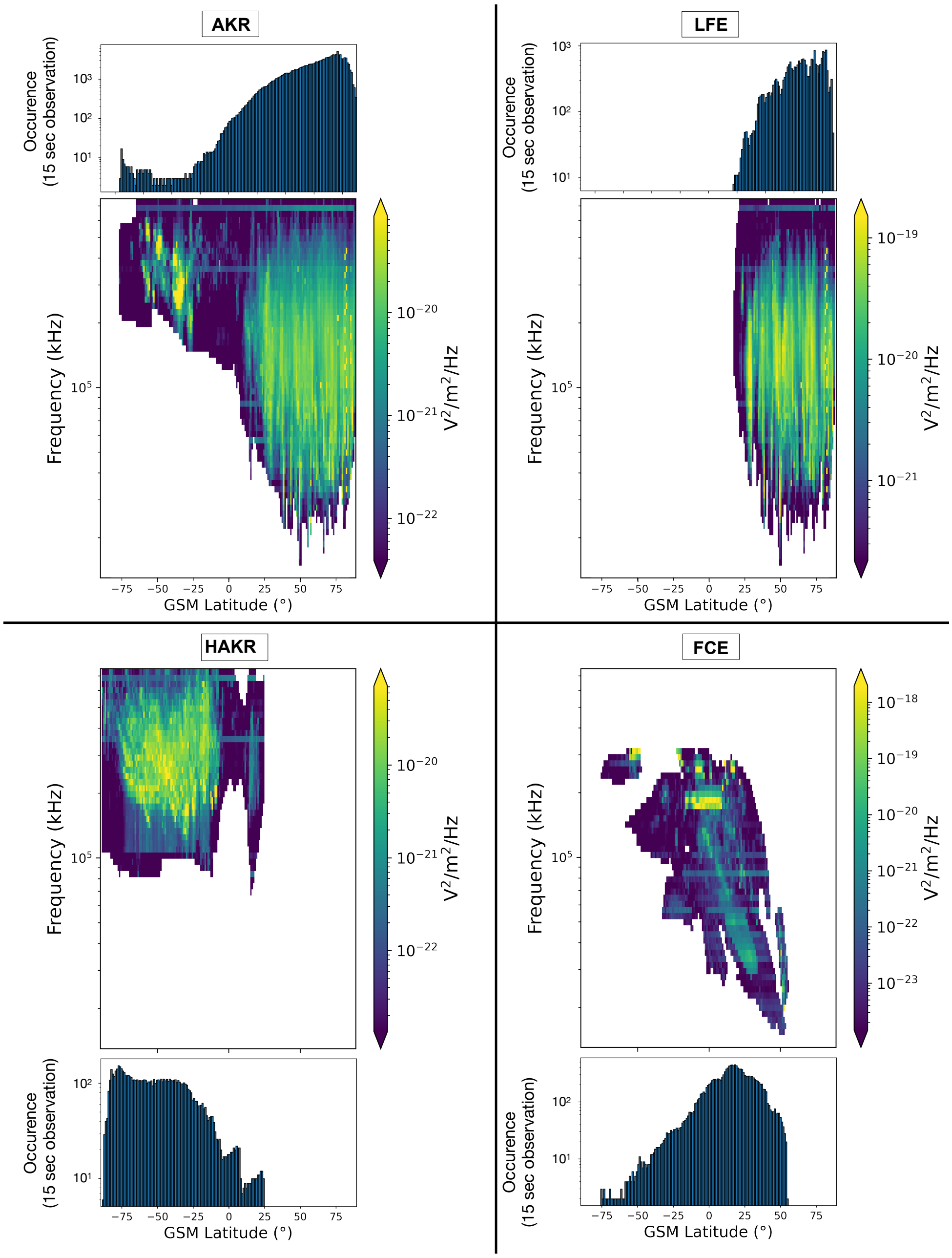

Figure 3: *Frequency vs. latitude intensity distribution for each feature of AKR emission (see Table 1) recorded by Polar from 1996/03/25 - 1996/05/10, in the GSM coordinates system. Colourbars are per-plot. Intensity is normalized to one Astronomical Unit. Next to each intensity distribution is plotted a* 1^o*-binned histogram of the latitudinal occurrence (number of 15-second observations).*

at mid to high northern latitudes, no LFE in the south and very little AKR at mid to high southern latitudes) is due to the orbits of *Polar* (see Figure 1). During the ~ 60 orbits studied here (~ 45 days), when *Polar* is in the southern hemisphere, it is also very close to the planet (less than 2 R_E). This gives some observation constraints.

Since almost only HAKR is visible when the spacecraft is in the southern hemisphere, it means that when the observer is very close to the pole (all HAKR emission visible at a distance < 4 R_E) only the higher frequency sources of the AKR ($> 150 - 200$ kHz) are visible, while the lower frequency emissions are not beamed in the observer directions. Indeed, radio waves cannot propagate in the planet direction since the electron cyclotron frequency f_{ce}, proportional to the magnetic field and a cutoff frequency of the CMI emissions, is increasing with decreasing altitude.

Regarding the AKR and the LFE, none are seen in the southern hemisphere, i.e. close to the planet. All AKR and LFE are observed when the spacecraft is at a distance > 3 R_E and > 4 R_E, respectively. (Note that the AKR emissions observed in the southern hemisphere represent a single event (occurrence $< 1\%$), and is therefore statistically irrelevant. This event is most likely a mislabelling of HAKR emission as AKR).

In the hemispheres where emissions are observed, we can see clear trends. For example, at latitudes close to 0°, we observe for AKR (top-left panel), LFE (top-right panel), and HAKR (bottom-left panel) a decrease in the maximal frequency and an increase in the minimal frequency reach by the emissions (from $\pm(25-30)°$ latitude) when approaching equatorial latitude.

Finally, the FCE (bottom-right panel) emission type is only observed when we are close to the perigee, i.e, when *Polar* is very close to the planet, therefore very close to the sources of the radio emissions. Comparing to the AKR (top-left panel) and HAKR (bottom-left panel) distributions, the FCE emissions are observed at the low frequency edge of the AKR and HAKR distributions

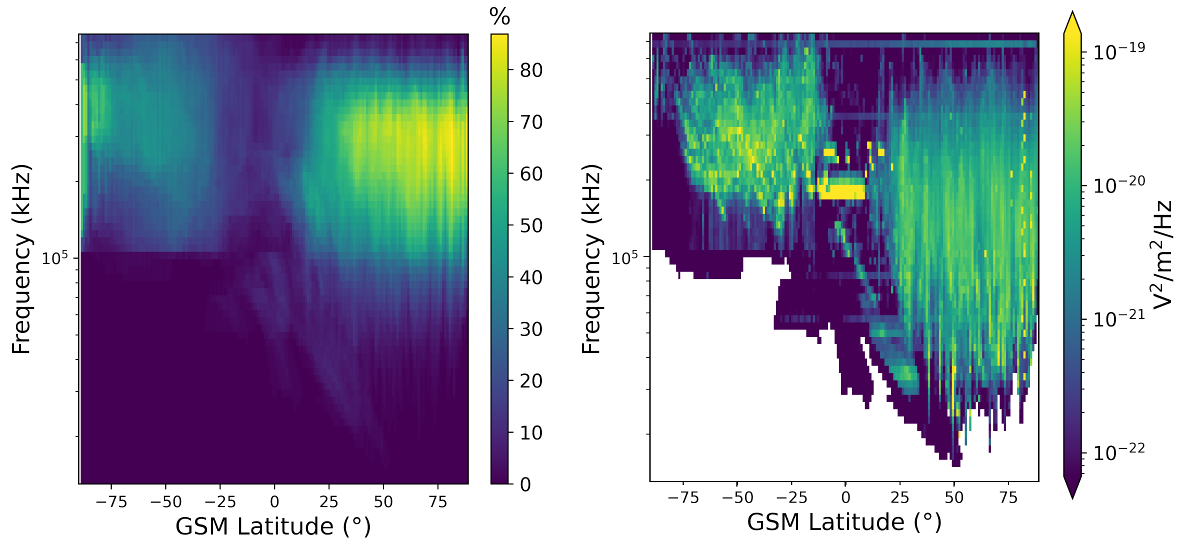

Figure 4: *Frequency vs. latitude occurrence (left) and intensity (right) distribution in the GSM coordinates system, for the AKR, HAKR and FCE emissions recorded by Polar from 1996/03/25 - 1996/05/10. Colourbars are per-plot. Intensity is normalized to one Astronomical Unit.*

The AKR, HAKR and FCE panels in Figure 3 are very complementary, so we used the catalogue to create a mask comprising these three components (the LFE component being included in the AKR component). Figure 4 displays a summary of the frequency vs. latitude occurrence (left) and intensity (right) distributions for these three components. The occurrence distribution is obtained by dividing the number of emissions observed in each latitude-frequency bin by the number of *Polar* observations in each of these bins.

On this figure, one can clearly see the area where almost no emission is visible, between ~ 20 and -20^o latitude, except for some FCE type emissions, corresponding to crossed (or near-by) sources (see Figure 3, FCE panels). This zone where no emission is observed can be explained by the orbits of *Polar*, which, during transits at latitudes close to 0°, is close to its perigee (see Figure 1). As a result, the spacecraft passes through the so-called equatorial shadow zone (Gurnett, 1974; Lamy et al., 2010; Morioka et al., 2011), where no more radio emissions are visible due to the emission geometry of the radio waves (along the edges of a hollow cone) and refraction effect on the plasmasphere. This equatorial shadow zone is also visible in Figure 1 (left panel), where we notice that on almost all orbits the integrated intensity is very low, or even non-existent, near the equator. Of course this shadow zone is frequency dependent, since the beaming direction as well as the refraction on the plasmasphere depends on the frequency, which is visible in Figure 4 (left panel), where the decrease in occurrence near the equator is not visible at the same latitude for each frequency.

The left panel of Figure 4 provides a better understanding of the occurrence of the AKR emissions. This allows us to determine statistically that the most regularly observed emissions are those in the $\sim$ 200-400 kHz frequency range (occurrence $> 80\%$). However, if we compare this with the emission intensity distribution, at least in the northern hemisphere, we can see that on average the most intense emissions are found at lower frequencies, corresponding to the LFE emissions (see Figure 3). In the southern hemisphere, we also find that the most intense emissions are located at lower frequencies than the bulk of the maximum occurrence. However, it is more difficult to make assumptions, as emissions in this latitude range are only seen at very close range.

6 Perspectives

To further the statistical study of the frequency vs. latitude distribution of the AKR, the catalogue should be extended until the end of the *Polar*/PWI observations (1997 September 16$^{\text{th}}$), in order to increase (1) the overall statistics by the number of features in the catalogue and (ii) the visibility in the Southern hemisphere for the AKR and LFEs and in the Northern hemisphere for the HAKR. This $\sim$ 45-day catalogue could be used as a basis for future machine learning approaches for automatic detection.

The latitudinal distribution using the catalogue extension could be supplemented with Wind/Waves data using the AKR selection technique of Waters et al. (2022). Both dataset are very complementary in term of latitude and local time coverage (see Figure 1 of Waters et al., 2022, for a distribution of AKR intensity as a function of latitude vs. local time), which will allow us to probe the entirety of the Earth's magnetosphere regions.

Understanding the latitudinal distributions of the AKR will allow us to better constrain the visibility effects of the AKR, and to compare them to other planets (such as Louis et al. (2021) for Jupiter, Lamy et al. (2008) for Saturn, see also Lamy et al. (2023), this issue) and to make predictions for observations of, e.g., Uranus or exoplanets.

Acknowledgments

C. K. Louis', C. M. Jackman's and A. R. Fogg's work at the Dublin Institute for Advanced Studies was funded by the Science Foundation Ireland Grant 18/FRL/6199. K. D. Smith's work was supported by SCOSTEP/PRESTO. A. R. Fogg's work was also supported by Irish Research Council Government of Ireland Postdoctoral Fellowship GOIPD/2022/782. C. K. Louis thanks A. Boudouma for his functions and routines for reading and working with the TFCat catalogues, and W. S. Kurth for his help in finding the *Polar* data.

References

Benson R. F., Calvert W., 1979, ISIS 1 observations at the source of Auroral Kilometric Radiation, *Geophysical Research Letters*, *6, 479*

Benson R. F., Calvert W., Klumpar D. M., 1980, Simultaneous wave and particle observations in the Auroral Kilometric Radiation source region, *Geophysical Research Letters*, *7, 959*

Calvert W., 1981, The auroral plasma cavity, *Geophysical Research Letters*, *8, 919*

Cecconi B., Louis C. K., Bonnin X., Loh A., Taylor M. B., 2023, Time-Frequency Catalogue: JSON Implementation and Python library, *Frontiers in Astronomy and Space Sciences*, *9*

Dunckel N., Ficklin B., Rorden L., Helliwell R. A., 1970, Low-frequency noise observed in the distant magnetosphere with OGO 1, *Journal of Geophysical Research*, *75, 1854*

Ergun R. E., et al., 1998, FAST satellite wave observations in the AKR source region, *Geophysical Research Letters*, *25, 2061*

Fogg A. R., Jackman C. M., Waters J. E., Bonnin X., Lamy L., Cecconi B., Issautier K., Louis C. K., 2022, Wind/WAVES Observations of Auroral Kilometric Radiation: Automated Burst Detection and Terrestrial Solar Wind - Magnetosphere Coupling Effects, *Journal of Geophysical Research (Space Physics)*, *127, e30209*

Green J. L., Gurnett D. A., Hoffman R. A., 1979, A correlation between Auroral Kilometric Radiation and inverted V electron precipitation, *Journal of Geophysical Research*, *84, 5216*

Gurnett D. A., 1974, The Earth as a radio source: Terrestrial kilometric radiation, *Journal of Geophysical Research*, *79, 4227*

Gurnett D. A., et al., 1995, The Polar Plasma Wave Instrument, *Space Science Reviews*, *71, 597*

Hilgers A., 1992, The auroral radiating plasma cavities, *Geophysical Research Letters*, *19, 237*

Huff R. L., Calvert W., Craven J. D., Frank L. A., Gurnett D. A., 1988, Mapping of Auroral Kilometric Radiation sources to the aurora, *Journal of Geophysics Research*, *93, 11445*

Johnson M. T., Wygant J. R., Cattell C., Mozer F. S., Temerin M., Scudder J., 2001, Observations of the seasonal dependence of the thermal plasma density in the Southern Hemisphere auroral zone and polar cap at 1 R_E, *Journal of Geophysical Research*, *106, 19023*

Lamy L., Zarka P., Cecconi B., Prangé R., Kurth W. S., Gurnett D. A., 2008, Saturn kilometric radiation: Average and statistical properties, *Journal of Geophysical Research (Space Physics)*, *113, A07201*

Lamy L., Zarka P., Cecconi B., Prangé R., 2010, Auroral kilometric radiation diurnal, semidiurnal, and shorter-term modulations disentangled by Cassini, *Journal of Geophysical Research (Space Physics)*, *115, A09221*

Lamy L., Louis C. K., Waters J. E., 2023, Comparative visibility of planetary auroral radio emissions and implications for the search for exoplanets, *in Planetary, Solar and Heliospheric Radio Emissions IX, eds Louis, C. K. and Jackman, C. M. and Fischer, G. and Sulaiman, A. H. and Zucca, P.*, DIAS and TCD, doi:10.25546/103091

Le Queau D., Pellat R., Roux A., 1984a, Direct generation of the Auroral Kilometric Radiation by the maser synchrotron instability: An analytical approach, *Physics of Fluids*, *27, 247*

Le Queau D., Pellat R., Roux A., 1984b, Direct generation of the Auroral Kilometric Radiation by the maser synchrotron instability: Physical mechanism and parametric study, *Journal of Geophysical Research*, *89, 2831*

Louis C. K., Zarka P., Dabidin K., Lampson P. A., Magalhães F. P., Boudouma A., Marques M. S., Cecconi B., 2021, Latitudinal Beaming of Jupiter's Radio Emissions From Juno/Waves Flux Density Measurements, *Journal of Geophysical Research (Space Physics)*, *126, e29435*

Louis C. K., et al., 2022a, SPACE Labelling Tool Version 2.0.0 (v2.0.0) [Code], doi:10.5281/zenodo.6886528, `https://doi.org/10.5281/zenodo.6886528`

Louis C., et al., 2022b, The "SPectrogram Analysis and Cataloguing Environment" (SPACE) labelling tool, *Frontiers in Astronomy and Space Sciences*, *9, 1001166*

Morioka A., et al., 2007, Dual structure of auroral acceleration regions at substorm onsets as derived from Auroral Kilometric Radiation spectra, *Journal of Geophysical Research (Space Physics)*, *112, A06245*

Morioka A., et al., 2011, On the simultaneity of substorm onset between two hemispheres, *Journal of Geophysical Research (Space Physics)*, *116, A04211*

Morioka A., Miyoshi Y., Kasaba Y., Sato N., Kadokura A., Misawa H., Miyashita Y., Mann I., 2014, Substorm onset process: Ignition of auroral acceleration and related substorm phases, *Journal of Geophysical Research (Space Physics)*, *119, 1044*

Mutel R. L., Gurnett D. A., Christopher I. W., Pickett J. S., Schlax M., 2003, Locations of Auroral Kilometric Radiation bursts inferred from multispacecraft wideband Cluster VLBI observations. 1: Description of technique and initial results, *Journal of Geophysical Research (Space Physics)*, *108, 1398*

Mutel R., Gurnett D., Christopher I., 2004, Spatial and temporal properties of AKR burst emission derived from Cluster WBD VLBI studies, *Annales Geophysicae*, *22, 2625*

Mutel R. L., Christopher I. W., Pickett J. S., 2008, Cluster multispacecraft determination of AKR angular beaming, *Geophysical Research Letters*, *35, L07104*

Pritchett P. L., 1986, Cyclotron maser radiation from a source structure localized perpendicular to the ambient magnetic field, *Journal of Geophysical Research*, *91, 13569*

Russell C. T., Snare R. C., Means J. D., Pierce D., Dearborn D., Larson M., Barr G., Le G., 1995, The GGS/POLAR magnetic fields investigation, *Space Science Reviews*, *71, 563*

Smith K. D., Louis C. K., Jackman C. M., Fogg A. R., O'Dwyer E., Waters J. E., Granroth L. J., 2022a, Catalogue of Auroral Kilometric Radiations (AKR) observed by the Polar spacecraft, doi:10.5281/zenodo.7260994, `https://doi.org/10.5281/zenodo.7260994`

Smith K. D., Louis C. K., Jackman C. M., Fogg A. R., O'Dwyer E., Waters J. E., Granroth L. J., 2022b, Polar / Plasma Waves Investigation processed dataset and ephemeris used to produced the Smith et al. (2022) catalogue (doi:10.5281/zenodo.7260994), doi:10.5281/zenodo.7589413, `https://doi.org/10.5281/zenodo.7589412`

Treumann R. A., 2006, The electron-cyclotron maser for astrophysical application, *Astronomy & Astrophysics Review*, *13, 229*

Treumann R. A., Baumjohann W., 2020, Auroral Kilometric Radiation and electron pairing, *Frontiers in Physics*, *8, 386*

Voots G. R., Gurnett D. A., Akasofu S. I., 1977, Auroral Kilometric Radiation as an indicator of auroral magnetic disturbances, *Journal of Geophysical Research*, *82, 2259*

Waters J. E., Jackman C. M., Lamy L., Cecconi B., Whiter D. K., Bonnin X., Issautier K., Fogg A. R., 2021, Empirical selection of Auroral Kilometric Radiation during a multipoint remote observation with Wind and Cassini, *Journal of Geophysical Research (Space Physics)*, *126, e29425*

Waters J. E., et al., 2022, A Perspective on Substorm Dynamics Using 10 Years of Auroral Kilometric Radiation Observations From Wind, *Journal of Geophysical Research (Space Physics)*, *127, e30449*

Wu C. S., 1985, Kinetic cyclotron and synchrotron maser instabilities - Radio emission processes by direct amplification of radiation, *Space Science Reviews*, *41, 215*

Wu C. S., Lee L. C., 1979, A theory of the terrestrial kilometric radiation., *Astrophysical Journal*, *230, 621*

Zhao W., Liu S., Zhang S., Zhou Q., Yang C., He Y., Gao Z., Xiao F., 2019, Global Occurrences of Auroral Kilometric Radiation Related to Suprathermal Electrons in Radiation Belts, *Geophysical Research Letters*, *46, 7230*